

System size dependence of associated yields in hadron-triggered jets

B. I. Abelev⁸, M. M. Aggarwal³⁰, Z. Ahammed⁴⁷, B. D. Anderson¹⁸,
D. Arkhipkin¹², G. S. Averichev¹¹, J. Balewski²², O. Barannikova⁸,
L. S. Barnby², J. Baudot¹⁶, S. Baumgart⁵², D. R. Beavis³, R. Bellwied⁵⁰,
F. Benedetto²⁷, M. J. Betancourt²², R. R. Betts⁸, A. Bhasin¹⁷, A. K. Bhati³⁰,
H. Bichsel⁴⁹, J. Bielcik¹, J. Bielcikova¹, B. Biritz⁶, L. C. Bland³,
M. Bombara², B. E. Bonner³⁶, M. Botje²⁷, J. Bouchet¹⁸, E. Braidot²⁷,
A. V. Brandin²⁵, E. Bruna⁵², S. Bueltmann²⁹, T. P. Burton², M. Bystersky¹,
X. Z. Cai⁴⁰, H. Caines⁵², M. Calderón de la Barca Sánchez⁵, O. Catu⁵²,
D. Cebra⁵, R. Cendejas⁶, M. C. Cervantes⁴², Z. Chajec²⁸, P. Chaloupka¹,
S. Chattopadhyay⁴⁷, H. F. Chen³⁸, J. H. Chen¹⁸, J. Y. Chen⁵¹, J. Cheng⁴⁴,
M. Cherney⁹, A. Chikanian⁵², K. E. Choi³⁴, W. Christie³, R. F. Clarke⁴²,
M. J. M. Coddington¹, R. Corliss²², T. M. Cormier⁵⁰, M. R. Cosentino³⁷,
J. G. Cramer⁴⁹, H. J. Crawford⁴, D. Das⁵, S. Dash¹, M. Daugherty⁴³,
L. C. De Silva⁵⁰, T. G. Dedovich¹¹, M. DePhillips³, A. A. Derevschikov³²,
R. Derradi de Souza⁷, L. Didenko³, P. Djawotho⁴², S. M. Dogra¹⁷, X. Dong²¹,
J. L. Drachenberg⁴², J. E. Draper⁵, F. Du⁵², J. C. Dunlop³,
M. R. Dutta Mazumdar⁴⁷, W. R. Edwards²¹, L. G. Efimov¹¹, E. Elhalluli²,
M. Elnimr⁵⁰, V. Emelianov²⁵, J. Engelage⁴, G. Eppley³⁶, B. Erazmus⁴¹,
M. Estienne¹⁶, L. Eun³¹, P. Fachini³, R. Fatemi¹⁹, J. Fedorisin¹¹, A. Feng⁵¹,
P. Filip¹², E. Finch⁵², V. Fine³, Y. Fisyak³, C. A. Gagliardi⁴², L. Gaillard²,
D. R. Gangadharan⁶, M. S. Ganti⁴⁷, E. J. Garcia-Solis⁸, Geromitsos⁴¹,
F. Geurts³⁶, V. Ghazikhanian⁶, P. Ghosh⁴⁷, Y. N. Gorbunov⁹, A. Gordon³,
O. Grebenyuk²¹, D. Grosnick⁴⁶, B. Grube³⁴, S. M. Guertin⁶,
K. S. F. F. Guimaraes³⁷, A. Gupta¹⁷, N. Gupta¹⁷, W. Guryn³, B. Haag⁵,
T. J. Hallman³, A. Hamed⁴², J. W. Harris⁵², W. He¹⁵, M. Heinz⁵²,
S. Heppelmann³¹, B. Hippolyte¹, A. Hirsch³³, E. Hjort²¹, A. M. Hoffmann²²,
G. W. Hoffmann⁴³, D. J. Hofman⁸, R. S. Hollis⁸, H. Z. Huang⁶,
T. J. Humanic²⁸, L. Huo⁴², G. Igo⁶, A. Iordanova⁸, P. Jacobs²¹,
W. W. Jacobs¹⁵, P. Jakl¹, C. Jena¹³, F. Jin⁴⁰, C. L. Jones²², P. G. Jones²,
J. Joseph¹⁸, E. G. Judd⁴, S. Kabana⁴¹, K. Kajimoto⁴³, K. Kang⁴⁴,
J. Kapitan¹, D. Keane¹⁸, A. Kechechyan¹¹, D. Kettler⁴⁹, V. Yu. Khodyrev³²,
D. P. Kikola²¹, J. Kiryluk²¹, A. Kisiel²⁸, S. R. Klein²¹, A. G. Knospe⁵²,
A. Kocoloski²², D. D. Koetke⁴⁶, M. Kopytine¹⁸, W. Korsch¹⁹, L. Kotchenda²⁵,
V. Kouchpil¹, P. Kravtsov²⁵, V. I. Kravtsov³², K. Krueger¹, M. Krus¹,
C. Kuhn¹⁶, L. Kumar³⁰, P. Kurnadi⁶, M. A. C. Lamont³, J. M. Landgraf³,
S. LaPointe⁵⁰, J. Lauret³, A. Lebedev³, R. Lednicky¹², C-H. Lee³⁴, J. H. Lee³,
W. Leight²², M. J. LeVine³, Li⁵¹, C. Li³⁸, Y. Li⁴⁴, G. Lin⁵²,
S. J. Lindenbaum²⁶, M. A. Lisa²⁸, F. Liu⁵¹, J. Liu³⁶, L. Liu⁵¹, T. Ljubicic³,
W. J. Llope³⁶, R. S. Longacre³, W. A. Love³, Y. Lu³⁸, T. Ludlam³,
G. L. Ma⁴⁰, Y. G. Ma⁴⁰, D. P. Mahapatra¹³, R. Majka⁵², O. I. Mall⁵,
L. K. Mangotra¹⁷, R. Manweiler⁴⁶, S. Margetis¹⁸, C. Markert⁴³, H. S. Matis²¹,
Yu. A. Matulenko³², T. S. McShane⁹, A. Meschanin³², R. Milner²²,

N. G. Minaev³², S. Mioduszewski⁴², A. Mischke²⁷, J. Mitchell³⁶,
 B. Mohanty⁴⁷, D. A. Morozov³², M. G. Munhoz³⁷, B. K. Nandi¹,
 C. Natrass⁵², T. K. Nayak⁴⁷, J. M. Nelson², P. K. Netrakanti³³, M. J. Ng⁴,
 L. V. Nogach³², S. B. Nurushev³², G. Odyniec²¹, A. Ogawa³, H. Okada³,
 V. Okorokov²⁵, D. Olson²¹, M. Pachr¹, B. S. Page¹⁵, S. K. Pal⁴⁷, Y. Pandit¹⁸,
 Y. Panebratsev¹¹, T. Pawlak⁴⁸, T. Peitzmann²⁷, V. Perevoztchikov³,
 C. Perkins⁴, W. Peryt⁴⁸, S. C. Phatak¹³, M. Planinic⁵³, J. Pluta⁴⁸,
 N. Poljak⁵³, A. M. Poskanzer²¹, B. V. K. S. Potukuchi¹⁷, D. Prindle⁴⁹,
 C. Pruneau⁵⁰, N. K. Pruthi³⁰, P. R. Pujahari¹, J. Putschke⁵², R. Raniwala³⁵,
 S. Raniwala³⁵, R. L. Ray⁴³, R. Redwine²², R. Reed⁵, A. Ridiger²⁵,
 H. G. Ritter²¹, J. B. Roberts³⁶, O. V. Rogachevskiy¹¹, J. L. Romero⁵,
 A. Rose²¹, C. Roy⁴¹, L. Ruan³, M. J. Russcher²⁷, R. Sahoo⁴¹, I. Sakrejda²¹,
 T. Sakuma²², S. Salur²¹, J. Sandweiss⁵², M. Sarsour⁴², J. Schambach⁴³,
 R. P. Scharenberg³³, N. Schmitz²³, J. Seger⁹, I. Selyuzhenkov¹⁵, P. Seyboth²³,
 A. Shabetai¹⁶, E. Shahaliev¹¹, M. Shao³⁸, M. Sharma⁵⁰, S. S. Shi⁵¹,
 X-H. Shi⁴⁰, E. P. Sichtermann²¹, F. Simon²³, R. N. Singaraju⁴⁷, M. J. Skoby³³,
 N. Smirnov⁵², R. Snellings²⁷, P. Sorensen³, J. Sowinski¹⁵, H. M. Spinka¹,
 B. Srivastava³³, A. Stadnik¹¹, T. D. S. Stanislaus⁴⁶, D. Staszak⁶,
 M. Strikhanov²⁵, B. Stringfellow³³, A. A. P. Suaide³⁷, M. C. Suarez⁸,
 N. L. Subba¹⁸, M. Sumner¹, X. M. Sun²¹, Y. Sun³⁸, Z. Sun¹, B. Surrow²²,
 T. J. M. Symons²¹, A. Szanto de Toledo³⁷, J. Takahashi⁷, A. H. Tang³,
 Z. Tang³⁸, T. Tarnowsky³³, D. Thein⁴³, J. H. Thomas²¹, J. Tian⁴⁰,
 A. R. Timmins², S. Timoshenko²⁵, D. Tlusty¹, M. Tokarev¹¹, T. A. Trainor⁴⁹,
 V. N. Tram²¹, A. L. Trattner⁴, S. Trentalange⁶, R. E. Tribble⁴², O. D. Tsai⁶,
 J. Ulery³³, T. Ullrich³, D. G. Underwood¹, G. Van Buren³, M. van Leeuwen²⁷,
 A. M. Vander Molen²⁴, J. A. Vanfossen, Jr.¹⁸, R. Varma¹,
 G. M. S. Vasconcelos⁷, I. M. Vasilevski¹², A. N. Vasiliev³², F. Videbaek³,
 S. E. Vigdor¹⁵, Y. P. Viyogi¹³, S. Vokal¹¹, S. A. Voloshin⁵⁰, M. Wada⁴³,
 W. T. Waggoner⁹, M. Walker²², F. Wang³³, G. Wang⁶, J. S. Wang¹,
 Q. Wang³³, X. Wang⁴⁴, X. L. Wang³⁸, Y. Wang⁴⁴, G. Webb¹⁹, J. C. Webb⁴⁶,
 G. D. Westfall²⁴, C. Whitten Jr.⁶, H. Wieman²¹, S. W. Wissink¹⁵, R. Witt⁴⁵,
 Y. Wu⁵¹, W. Xie³³, N. Xu²¹, Q. H. Xu³⁹, Y. Xu³⁸, Z. Xu³, Yang¹, P. Yepes³⁶,
 I-K. Yoo³⁴, Q. Yue⁴⁴, M. Zawisza⁴⁸, H. Zbroszczyk⁴⁸, W. Zhan¹, S. Zhang⁴⁰,
 W. M. Zhang¹⁸, X. P. Zhang²¹, Y. Zhang²¹, Z. P. Zhang³⁸, Y. Zhao³⁸,
 C. Zhong⁴⁰, J. Zhou³⁶, R. Zoulkarneev¹², Y. Zoulkarneeva¹², J. X. Zuo⁴⁰

(STAR COLLABORATION)

¹Argonne National Laboratory, Argonne, Illinois 60439, USA

²University of Birmingham, Birmingham, United Kingdom

³Brookhaven National Laboratory, Upton, New York 11973, USA

⁴University of California, Berkeley, California 94720, USA

⁵University of California, Davis, California 95616, USA

⁶University of California, Los Angeles, California 90095, USA

⁷Universidade Estadual de Campinas, Sao Paulo, Brazil

⁸University of Illinois at Chicago, Chicago, Illinois 60607, USA

⁹Creighton University, Omaha, Nebraska 68178, USA

¹⁰Nuclear Physics Institute AS CR, 250 68 Řež/Prague, Czech Republic

¹¹Laboratory for High Energy (JINR), Dubna, Russia

- ¹²Particle Physics Laboratory (JINR), Dubna, Russia
¹³Institute of Physics, Bhubaneswar 751005, India
¹⁴Indian Institute of Technology, Mumbai, India
¹⁵Indiana University, Bloomington, Indiana 47408, USA
¹⁶Institut de Recherches Subatomiques, Strasbourg, France
¹⁷University of Jammu, Jammu 180001, India
¹⁸Kent State University, Kent, Ohio 44242, USA
¹⁹University of Kentucky, Lexington, Kentucky, 40506-0055, USA
²⁰Institute of Modern Physics, Lanzhou, China
²¹Lawrence Berkeley National Laboratory, Berkeley, California 94720, USA
²²Massachusetts Institute of Technology, Cambridge, MA 02139-4307, USA
²³Max-Planck-Institut für Physik, Munich, Germany
²⁴Michigan State University, East Lansing, Michigan 48824, USA
²⁵Moscow Engineering Physics Institute, Moscow Russia
²⁶City College of New York, New York City, New York 10031, USA
²⁷NIKHEF and Utrecht University, Amsterdam, The Netherlands
²⁸Ohio State University, Columbus, Ohio 43210, USA
²⁹Old Dominion University, Norfolk, VA, 23529, USA
³⁰Panjab University, Chandigarh 160014, India
³¹Pennsylvania State University, University Park, Pennsylvania 16802, USA
³²Institute of High Energy Physics, Protvino, Russia
³³Purdue University, West Lafayette, Indiana 47907, USA
³⁴Pusan National University, Pusan, Republic of Korea
³⁵University of Rajasthan, Jaipur 302004, India
³⁶Rice University, Houston, Texas 77251, USA
³⁷Universidade de Sao Paulo, Sao Paulo, Brazil
³⁸University of Science & Technology of China, Hefei 230026, China
³⁹Shandong University, Jinan, Shandong 250100, China
⁴⁰Shanghai Institute of Applied Physics, Shanghai 201800, China
⁴¹SUBATECH, Nantes, France
⁴²Texas A&M University, College Station, Texas 77843, USA
⁴³University of Texas, Austin, Texas 78712, USA
⁴⁴Tsinghua University, Beijing 100084, China
⁴⁵United States Naval Academy, Annapolis, MD 21402, USA
⁴⁶Valparaiso University, Valparaiso, Indiana 46383, USA
⁴⁷Variable Energy Cyclotron Centre, Kolkata 700064, India
⁴⁸Warsaw University of Technology, Warsaw, Poland
⁴⁹University of Washington, Seattle, Washington 98195, USA
⁵⁰Wayne State University, Detroit, Michigan 48201, USA
⁵¹Institute of Particle Physics, CCNU (HZNU), Wuhan 430079, China
⁵²Yale University, New Haven, Connecticut 06520, USA
⁵³University of Zagreb, Zagreb, HR-10002, Croatia

Abstract

We present results on the system size dependence of high transverse momentum di-hadron correlations at $\sqrt{s_{NN}} = 200$ GeV as measured by STAR at RHIC. Measurements in d+Au, Cu+Cu and Au+Au collisions reveal similar jet-like correlation yields at small angular separation ($\Delta\phi \sim 0$, $\Delta\eta \sim 0$) for all systems and centralities. Previous measurements have shown that the away-side yield is suppressed in heavy-ion collisions. We present measurements of the away-side suppression as a function of transverse momentum and centrality in Cu+Cu

and Au+Au collisions. The suppression is found to be similar in Cu+Cu and Au+Au collisions at a similar number of participants. The results are compared to theoretical calculations based on the parton quenching model and the modified fragmentation model. The observed differences between data and theory indicate that the correlated yields presented here will provide important constraints on medium density profile and energy loss model parameters.

Key words: parton energy loss, jet quenching, di-hadron fragmentation function, relativistic heavy-ion collisions

PACS: 25.75.-q, 25.75.Gz

One of the important early results from the experiments at RHIC is the observation of jet quenching in heavy-ion collisions. The suppression of high transverse momentum (p_T) particle production in inclusive hadron spectra [1, 2] and jet-like structures in di-hadron correlation measurements [3] indicates that partons originating from hard scatterings in the initial stages of the collisions interact strongly with the created medium.

Previous studies [4] investigated azimuthal correlations of high- p_T hadrons and showed that the suppression of the correlated away-side yield increases with centrality in Au+Au collisions. Various theoretical calculations [5, 6, 7, 8] of partonic energy loss in the medium have been used to derive medium properties like the transport coefficient \hat{q} . The energy loss of individual partons is also expected to depend on the path length through the medium in a way that is characteristic of the energy loss mechanism. For radiative energy loss, which is thought to be dominant for light quarks, the energy loss is expected to depend on L^2 , the square of the traversed path length, due to coherence effects [9, 10, 11]. For elastic energy loss, on the other hand, a linear dependence on L is expected. Prior results from RHIC have not established in detail the energy loss mechanism. Combined measurements of single-hadron and di-hadron suppression are sensitive to the path length dependence and can help determine which process dominates [12]. In addition, different implementations of the energy loss calculation use different path-length distributions and density profiles. The system-size dependence of away-side suppression is sensitive to these modeling parameters and will provide further constraints [13].

We present a systematic study of the near- ($\Delta\phi \sim 0$) and away-side ($|\Delta\phi| \sim \pi$) di-hadron correlated yields as a function of the number of participant nucleons (N_{part}). Data for three systems with different geometries (d+Au, Cu+Cu and Au+Au) at $\sqrt{s_{NN}} = 200$ GeV were collected by the STAR experiment at RHIC. A study of the hadron-triggered fragmentation functions in the three systems is also presented. Results from d+Au collisions are used as a reference without a hot medium. The d+Au data sample is preferred over the p+p data sample because it has significantly larger statistics. Earlier comparisons between p+p and d+Au collisions have established that jet suppression is a final state effect and is not present in d+Au collisions [14, 15, 16, 17].

This analysis is based on four data sets and includes 11.7 million minimum-

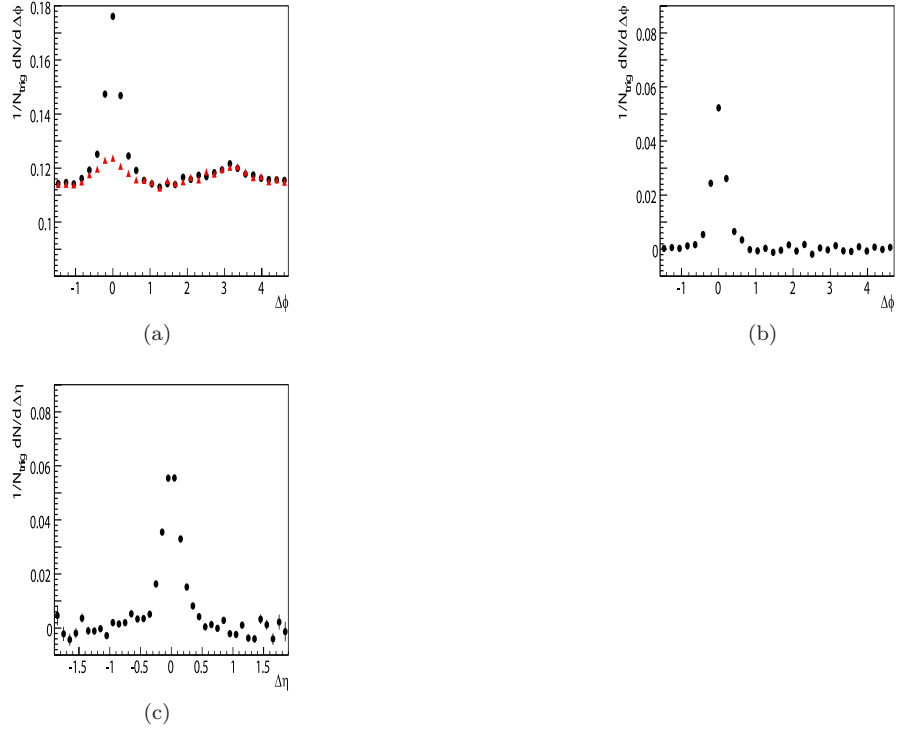


Figure 1: Di-hadron correlations in central (0-12%) Au+Au collisions: (a) $\Delta\phi$ correlations - small $\Delta\eta$ ($|\Delta\eta| < 0.7$) (black circles) and large $\Delta\eta$ ($0.7 < |\Delta\eta| < 1.7$) scaled to match the small $\Delta\eta$ result at large $\Delta\phi$ (red triangles), (b) $\Delta\phi$ subtracted distribution, (c) $\Delta\eta$ subtracted distributions; $4 < p_T^{trig} < 6$ GeV/c, $p_T^{assoc} > 3$ GeV/c.

bias d+Au events, 43.8 million minimum-bias Cu+Cu events, 25 million minimum-bias Au+Au events and 19 million Au+Au events collected using a central trigger. The central trigger uses the coincidence of two Zero Degree Calorimeters (ZDCs) and a multiplicity threshold in the Central Trigger Barrel [18] which selects the most central 0 – 12% of total geometric cross-section. In order to minimize the influence of the Time Projection Chamber (TPC) acceptance [19], only events with a reconstructed collision vertex with $|z_{vertex}| \leq 30$ cm are included in the analysis, where z_{vertex} represents the distance along the beam-line from the center of the detector.

The di-hadron correlations are formed using charged particles reconstructed in the TPC, within a pseudorapidity range of $-1 < \eta < 1$. High p_T trigger particles are selected and the $\Delta\eta \times \Delta\phi$ distribution of associated particles ($p_T^{assoc} < p_T^{trig}$) is constructed. An η , p_T and centrality dependent reconstruction efficiency correction is applied to obtain the associated particle yields. It is not necessary to apply the efficiency correction to trigger particles when calculating the correlated yields because the final result is normalised per trigger particle. The track reconstruction efficiency depends on the track density within the TPC and ranges from 89% (peripheral collisions) to 77% (central). The systematic uncertainty on the efficiency correction is estimated to be 5% and is strongly correlated across centralities and p_T bins for each data set, but not between data sets. particles is not necessary since

Pair acceptance corrections in $\Delta\phi$ and $\Delta\eta$ are computed using a mixed event technique. These corrections reflect the conditional probability of reconstructing two tracks with a specified relative kinematics. The dominant feature in the $\Delta\phi$ pair acceptance correction are the small gaps between the sectors of the TPC. The $\Delta\eta$ pair acceptance correction is of triangular shape, with a maximum of 1 at mid-rapidity and minimum of 0 at the limit of the pair acceptance $\Delta\eta = \pm 2$. The $\Delta\eta$ acceptance correction is not applied to the away-side yields.

Earlier results from STAR [20, 21] have shown that there is a finite associated yield on the near-side ($\Delta\phi \sim 0$) with large pseudorapidity separation $\Delta\eta$ (the “ridge”). Since the ridge properties are similar to those of the medium, it is appropriate to subtract this contribution in the present analysis. In order to extract the jet contribution to the near-side yield, the azimuthal correlation distribution for large $\Delta\eta$ separation ($0.7 < |\Delta\eta| < 1.7$) is subtracted from the distribution for small $\Delta\eta$ ($|\Delta\eta| < 0.7$). To account for the different $\Delta\eta$ window widths, the former distribution is scaled so that the two distributions match in the away-side region. This subtraction removes the $\Delta\eta$ -independent ridge contribution and the contributions from elliptic flow v_2 , which is also largely independent of η in the range considered [22]. Figure 1a shows central Au+Au distributions in the large (black) and small (red) $\Delta\eta$ regions, for trigger particles with transverse momentum $4 \text{ GeV}/c < p_T^{trig} < 6 \text{ GeV}/c$, and associated particles with p_T^{assoc} in the range $3 \text{ GeV}/c < p_T^{assoc} < p_T^{trig}$. The signal distribution after subtraction is shown in Fig. 1b.

An alternative way to extract the near-side associated yield is to use the $\Delta\eta$ -distribution, which is obtained by projecting the $\Delta\eta \times \Delta\phi$ correlations in the $|\Delta\phi| < 0.78$ region onto the $\Delta\eta$ axis. In this projection, the ridge yield

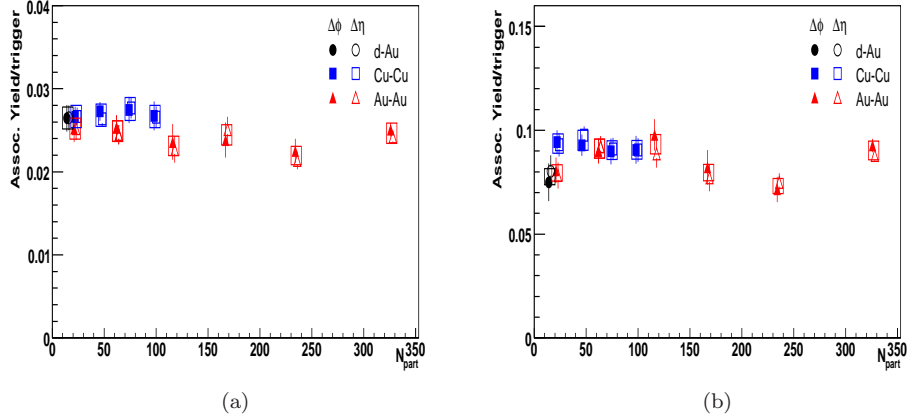


Figure 2: N_{part} dependence of the the near-side associated-particle yield for two trigger p_T ranges: (a) $4 \text{ GeV}/c < p_T^{trig} < 6 \text{ GeV}/c$, (b) $6 \text{ GeV}/c < p_T^{trig} < 10 \text{ GeV}/c$. For both panels $3 \text{ GeV}/c < p_T^{assoc} < p_T^{trig}$. The hollow symbols are horizontally offset for clarity.

and elliptic flow constitute a flat background which is determined by averaging the yield at large $|\Delta\eta| > 0.7$ and subtracted. Figure 1c shows a background subtracted $\Delta\eta$ projection with the same trigger conditions as Fig. 1a and Fig. 1b.

The near-side associated-particle yield, defined as

$$Y_{AA}^{near} = \int_{-0.7}^{0.7} d(\Delta\eta) \int_{-0.78}^{0.78} d(\Delta\phi) \frac{1}{N_{trig}} \frac{d^2 N_{corrected}}{d(\Delta\eta)d(\Delta\phi)} \quad (1)$$

is presented as a function of number of participant nucleons (N_{part}) in Fig. 2. The two methods produce results that are consistent with each other. The Cu+Cu and Au+Au near-side associated yields are consistent within errors for similar N_{part} . The near-side yields in heavy-ion collisions show no centrality dependence and within errors agree with those in d+Au, as seen also in previous studies [4]. The observed independence of the near-side associated yields on centrality indicates that in this p_T -range fragmentation is largely unmodified by the presence of the medium. Note that this does not necessarily imply that those partons do not lose energy, but rather that they fragment outside the medium after energy loss. In that case, the energy loss would reduce the number of trigger hadrons at a given p_T , but not change the associated particle distribution at intermediate to high p_T . The enhancement of associated particles at low p_T that has been reported earlier [20] could then be due to fragments of radiated gluons.

The choice of high- p_T trigger particles leads to a surface bias in the distribution of hard scattering points [13]. The away-side partons have longer path lengths through the medium and therefore will suffer higher energy losses

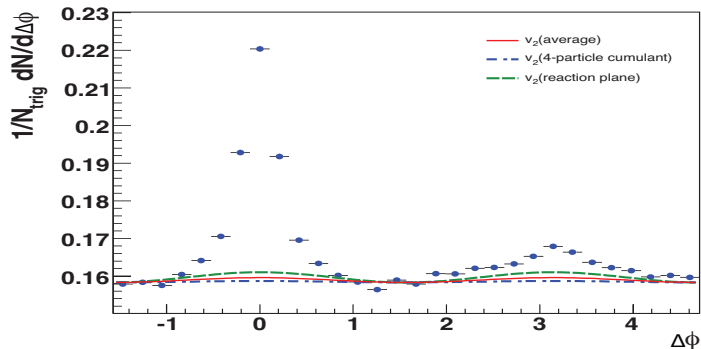


Figure 3: $\Delta\phi$ distribution in (0-12%) central Au+Au collisions used to extract the away-side yield, $4 \text{ GeV}/c < p_T^{trig} < 6 \text{ GeV}/c$, $3 \text{ GeV}/c < p_T^{assoc} < p_T^{trig}$, $|\Delta\eta| < 1.7$. The triangular pair acceptance correction in $\Delta\eta$ is not applied. The green line represents the elliptic flow modulated background using the values of v_2 calculated using the reaction plane method, the blue line uses the v_2 obtained using the 4-particle cumulant method. The red line uses the average value of v_2 .

that lead to away-side yield suppression. The study of the away-side yield suppression provides an important tool for determining the energy loss dependence on path length. The away-side associated-particle yield is measured by integrating the associated hadrons in the region $|\Delta\phi - \pi| < 1.3$, covering the azimuthal range of the away-side jet. A background subtraction is applied to remove the background which is correlated with the trigger particles through elliptic flow v_2 . The elliptic flow modulated background is described by $dN/d(\Delta\phi) = B \left(1 + 2\langle v_2^{trig} v_2^{assoc} \rangle \cos(2\Delta\phi) \right)$, and is illustrated in Fig. 3 for central collisions. The background is subtracted using the assumption that there is no jet contribution at the minimum of the distribution [23] — in this case at $|\Delta\phi| \sim 1$.

The amplitude of the background modulation is given by $\langle v_2^{trig} v_2^{assoc} \rangle \approx \langle v_2^{trig} \rangle \langle v_2^{assoc} \rangle$ which is measured in STAR using a number of different methods [24]. For the Au+Au collisions, the nominal value of v_2 for the background subtraction was the average between the four-particle cumulant and the reaction plane measurements of v_2 . In the Cu+Cu case, the nominal value is the average between the v_2 results obtained using two methods. The first method is the reaction plane method using tracks in the Forward Time Projection Chamber [25]. The second method uses tracks in the TPC but subtracts the azimuthal correlations in p+p collisions to remove non-flow correlations. The systematic uncertainty associated with the background removal is estimated in both cases as the difference between the results given by each method and the nominal value.

The background subtracted away-side yields are used to compute the sup-

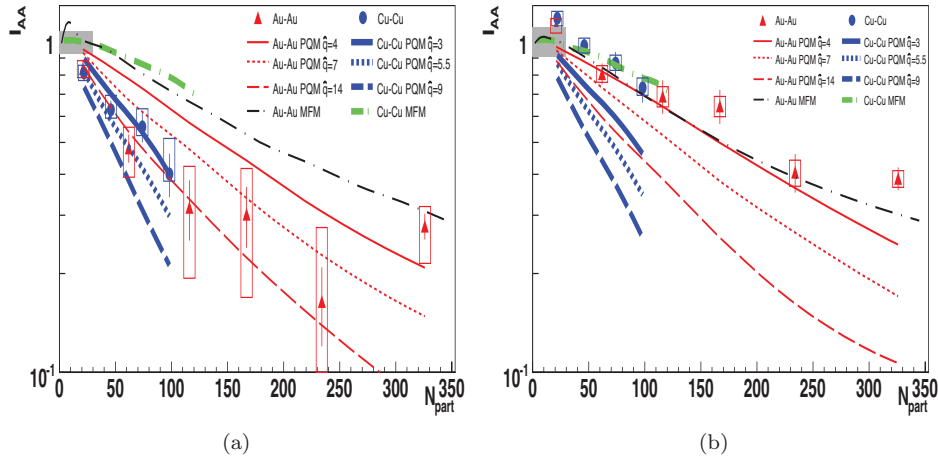


Figure 4: N_{part} dependence of the away-side associated-particle yield for two trigger p_T ranges: (a) $4 \text{ GeV}/c < p_T^{trig} < 6 \text{ GeV}/c$ (b) $6 \text{ GeV}/c < p_T^{trig} < 10 \text{ GeV}/c$. For both panels $3 \text{ GeV}/c < p_T^{assoc} < p_T^{trig}$. The error bars represent statistical errors and the boxes represent the point-to-point systematic errors. The gray band represents the correlated error due to the statistical error in the d+Au data. The lines represent calculations in PQM and MFM models. The values of \hat{q} are expressed in GeV^2/fm .

pression factor $I_{AA} = Y_{AA}^{away} / Y_{dAu}^{away}$, where $Y_{AA(dAu)}^{away}$ is the away-side di-hadron correlation strength in heavy-ion and d+Au collisions, respectively. Figure 4 shows the results for I_{AA} as a function of number of participants for Cu+Cu and Au+Au collisions. The away-side yield suppression increases with N_{part} , as expected. The Cu+Cu results show a similar suppression (I_{AA}) at the same number of participants as the Au+Au results, despite possible differences in density and path length distributions.

Figure 4 also shows two model calculations implementing the same kinematic cuts as our analysis.¹ One calculation, the Parton Quenching Model (PQM) [5, 26], uses the Salgado-Wiedemann quenching weights [27] with a Glauber-overlap geometry in which the local density scales with the local density of binary collisions ρ_{coll} . The other model uses a next-to-leading order QCD calculation with modified fragmentation functions from a higher-twist formalism [28] and a hard-sphere geometry where the density scales with the local participant density ρ_{part} [6]. We refer to this model as the Modified Fragmentation Model (MFM). The MFM authors used previous data on the suppression of high- p_T away-side yields in central Au+Au collisions [4] to tune their model. The PQM authors present 3 calculations, based on 3 values of \hat{q} in central

¹The model calculations use p+p as the reference, which is expected to be equivalent to the d+Au measurement used in the data.

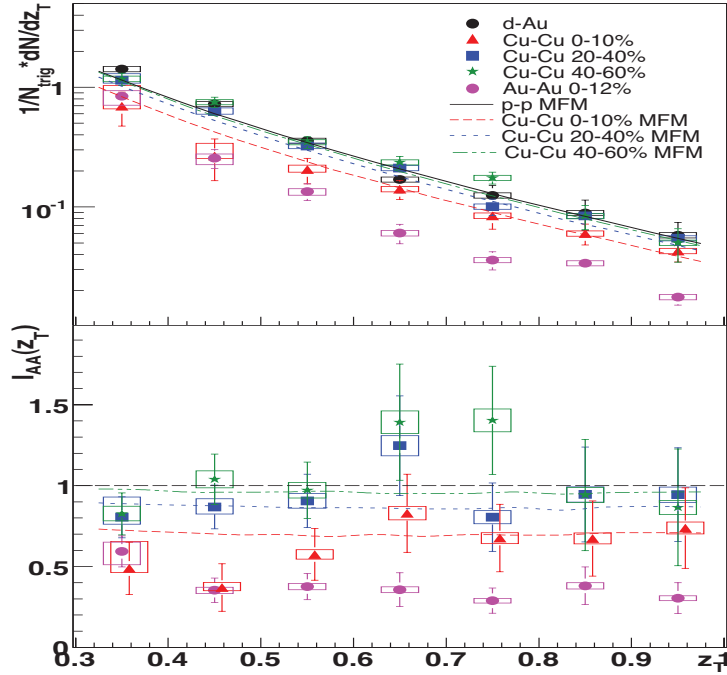


Figure 5: Away-side associated particle distribution and I_{AA} for $6 < p_T^{trig} < 10$ GeV/c. The error bars represent statistical errors and the boxes represent the total systematic errors. The lines represent calculations in MFM model.

collisions, indicated by different line styles in the figure.

For the lower trigger selection, $4 \text{ GeV}/c < p_T^{trig} < 6 \text{ GeV}/c$, the Modified Fragmentation Model predicts a smaller suppression than observed in the data, whereas PQM cannot explain Cu+Cu or Au+Au results in a consistent fashion. The disagreement between the models and the data suggests that the effect of kinematic limits (energy loss cannot be larger than the jet energy) and non-perturbative effects, which are not explicitly treated in the model, are significant in this p_T -range. For the higher trigger p_T range, $6 \text{ GeV}/c < p_T^{trig} < 10 \text{ GeV}/c$, a better agreement between the data and MFM is observed. There is an obvious difference between the system size dependence in the two models. While MFM obtains I_{AA} values that are independent on the system at a certain N_{part} , PQM shows a clear difference between the two systems for similar N_{part} , when using a common scaling of the medium density (represented by line styles in the figure). Further model studies are needed to clarify whether the different scaling behavior in MFM and PQM is mainly a result of the different quenching formalisms or rather due to differences between the medium density models.

In Figs. 2 and 4 we have presented results for a single selection of associated hadrons, $p_T^{assoc} > 3 \text{ GeV}/c$. A more differential measurement is pre-

sented in Fig. 5, which shows the away-side associated yield as a function of $z_T = p_T^{assoc}/p_T^{trig}$. The lower panel of Fig. 5 shows the z_T -dependence of I_{AA} . The away-side suppression is approximately independent of z_T in the measured range, indicating that the momentum distribution of fragments along the jet axis is not modified by energy loss. A possible explanation of the z_T -independent I_{AA} is that energy loss is large enough that partons which lose energy have such a soft fragment distribution that they do not contribute significantly to the away-side yield. The remaining away-side yield would then be dominantly from the fraction of partons that lost little or no energy due to a short path length (surface bias, tangential jets) or energy loss fluctuations. Also shown in Fig. 5 are calculations in the Modified Fragmentation Model [6], which agree with the results within the present statistical uncertainties.

In summary, we have presented a systematic study of di-hadron correlations of particles associated with high transverse momentum trigger hadrons. We have studied the jet-like correlations on the near-side ($\Delta\phi \sim 0$) and away-side ($\Delta\phi \sim \pi$) for d+Au, Cu+Cu and Au+Au collisions at $\sqrt{s_{NN}} = 200$ GeV/c. Near-side associated yields are equal within the experimental uncertainty for all the systems studied and independent of the number of participant nucleons (N_{part}). Away-side associated yields are suppressed in heavy-ion collisions with respect to the d+Au reference. The suppression increases with increasing N_{part} and shows no significant dependence on the collision system for a given N_{part} . The Parton Quenching Model [5, 26] does not describe the similarity of the away-side yields in the two collision systems at a given N_{part} , while the Modified Fragmentation Model [6, 28] describes this relatively well for the higher p_T triggers. Further comparison of these measurements to models may allow the extraction of the path length dependence of energy loss and whether elastic or radiative energy loss is dominant [12].

We thank the RHIC Operations Group and RCF at BNL, and the NERSC Center at LBNL and the resources provided by the Open Science Grid consortium for their support. This work was supported in part by the Offices of NP and HEP within the U.S. DOE Office of Science, the U.S. NSF, the Sloan Foundation, the DFG cluster of excellence ‘Origin and Structure of the Universe’, CNRS/IN2P3, RA, RPL, and EMN of France, STFC and EPSRC of the United Kingdom, FAPESP of Brazil, the Russian Ministry of Sci. and Tech., the NNSFC, CAS, MoST, and MoE of China, IRP and GA of the Czech Republic, FOM of the Netherlands, DAE, DST, and CSIR of the Government of India, the Polish State Committee for Scientific Research, and the Korea Sci. & Eng. Foundation.

References

- [1] K. Adcox et al. (PHENIX Collaboration), Phys. Rev. Lett. **88**, 022301 (2002).
- [2] C. Adler et al. (STAR Collaboration), Phys. Rev. Lett. **89**, 202301 (2002).

- [3] C. Adler et al. (STAR Collaboration), Phys. Rev. Lett. **90**, 082302 (2003).
- [4] J. Adams et al. (STAR Collaboration) , Phys. Rev. Lett. **97**, 162301 (2006).
- [5] C. Loizides, Eur. Phys. J. **C49**, 339 (2007).
- [6] X. N. Wang, Phys. Rev. Lett. **98**, 212301 (2007).
- [7] M. Gyulassy, P. Levai, I. Vitev, Nucl. Phys. **B571**, 197 (2000).
- [8] S. Wicks, W. Horowitz, M. Djordjevic and M. Gyulassy, Nucl. Phys. **A784**, 426 (2007).
- [9] R. Baier, Yu. L. Dokshitzer, S. Peigné and D. Schiff, Phys. Lett. **B345**, 277 (1995).
- [10] R. Baier, Yu. L. Dokshitzer, A. H. Mueller, S. Peigné and D. Schiff, Nucl. Phys. **B483**, 291 (1997).
- [11] R. Baier, Yu. L. Dokshitzer, A. H. Mueller, S. Peigné and D. Schiff, Nucl. Phys. **B484**, 265 (1997).
- [12] T. Renk, Phys. Rev. **C76**, 064905 (2007).
- [13] T. Renk and K. Eskola, Phys. Rev. **C75**, 054910 (2007).
- [14] B. B. Back et al. (PHOBOS Collaboration), Phys. Rev. Lett. **91**, 072302 (2003).
- [15] J. Adams et al. (STAR Collaboration), Phys. Rev. Lett. **91**, 072304 (2003).
- [16] S. S. Adler et al. (PHENIX Collaboration), Phys. Rev. Lett. **91**, 072303 (2003).
- [17] I. Arsene et al. (BRAHMS Collaboration), Phys. Rev. Lett. **91**, 072305 (2003).
- [18] K. H. Ackermann et al. (STAR Collaboration), Nucl. Instr. Meth. **A499**, 624 (2003).
- [19] M. Anderson et al., Nucl. Instrum. Meth. **A499**, 624 (2003).
- [20] J. Adams et al. (STAR Collaboration), Phys. Rev. Lett. **95**, 152301 (2005).
- [21] J. Adams et al. (STAR Collaboration), Phys. Rev. **C73**, 064907 (2006).
- [22] C. Adler *et al.* (STAR Collaboration), Phys. Rev. C **66**, 034904 (2002).
- [23] N.N. Ajitanand et al., Phys. Rev. **C72**, 011902 (2005).
- [24] B. I. Abelev et al. (STAR Collaboration), Phys. Rev. **C75**, 054906 (2007).
- [25] K. H. Ackermann et al., Nucl. Instrum. Meth. **A 499**, 713 (2003).

- [26] A. Dainese, C. Loizides, G. Paic, Eur. Phys. J. **C38**, 461 (2005).
- [27] C. A. Salgado, U. A. Wiedemann, Phys. Rev. **D68**, 014008 (2003).
- [28] X. N. Wang, Phys. Lett. **B595**, 165 (2004).